A Theoretical Model of Slow Wave Regulation Using Voltage-Dependent Synthesis of Inositol 1,4,5-Trisphosphate

Mohammad S. Imtiaz,* David W. Smith,† and Dirk F. van Helden*
*The Neuroscience Group, The Faculty of Medicine & Health Sciences, and †School of Engineering, The University of Newcastle, NSW 2308, Australia

ABSTRACT

A qualitative mathematical model is presented that examines membrane potential feedback on synthesis of inositol 1,4,5-trisphosphate (IP_3), and its role in generation and modulation of slow waves. Previous experimental studies indicate that slow waves show voltage dependence, and this is likely to result through membrane potential modulation of IP_3. It is proposed that the observed response of the tissue to current pulse, pulse train, and maintained current injection can be explained by changes in IP_3, modulated through a voltage-IP_3 feedback loop. Differences underlying the tissue responses to current injections of opposite polarities are shown to be due to the sequence of events following such currents. Results from this model are consistent with experimental findings and provide further understanding of these experimental observations. Specifically, we find that membrane potential can induce, abolish, and modulate slow wave frequency by altering the excitability of the tissue through the voltage-IP_3 feedback loop.

INTRODUCTION

Slow waves are rhythmic electrical depolarizations that initiate and control mechanical activity of many smooth muscles (Bolton, 1971; Daniel et al., 1994; Prosser and Mangel, 1982; Sanders, 1996; Tomita, 1981). The mechanism responsible for the generation of slow waves involves inositol 1,4,5-trisphosphate (IP_3)-induced Ca^{2+} release (IICR) and calcium-induced calcium release (CICR) from IP_3-operated intracellular Ca^{2+} stores (Hashitani et al., 1996; Liu et al., 1995; Suzuki and Hirst, 1999; van Helden et al., 2000). The resultant Ca^{2+} increases in the subplasmalemma space then activate Ca^{2+}-sensitive inward currents across the plasmalemma that result in slow wave depolarizations.

While it is accepted that IP_3 oscillations are not necessary for Ca^{2+} oscillations (Berridge, 1993a; Bird et al., 1997), it has been shown that IP_3 oscillations do occur in many cell types (Hirose et al., 1999). Two basic feedback mechanisms have been postulated to modulate IP_3 synthesis; one based on cytosolic calcium (Harootunian et al., 1991a, b) and the other on membrane potential (see below). In various cell types the first mechanism, Ca^{2+} feedback on IP_3 synthesis, has not been found to be operative (Bird et al., 1997). In the tissue of the present study, guinea-pig gastric smooth muscle, membrane potential is likely to be a significant modulator of IP_3 (Suzuki and Hirst, 1999; van Helden et al., 2000). In this paper we will study the role of membrane potential feedback on IP_3 synthesis and its role in regulation of Ca^{2+} release and slow waves.

Submitted February 21, 2002, and accepted for publication June 3, 2002.

Address reprint requests to Dirk F. van Helden, University Drive, Medical Sciences Building, Callaghan, NSW 2308, Australia. Tel: 61-2-49 215626; Fax: 61-2-49 217406; E-mail: hpdvh@mail.newcastle.edu.au.

0006-3495/02/10/1877/14 $2.00

In guinea-pig jejunal longitudinal smooth muscle, depolarization has been shown to increase synthesis of IP_3 (Best and Bolton, 1986). It has also been shown that hyperpolarization reduces the rate of IP_3 synthesis (Ganitkevich and Isenberg, 1996; Itoh et al., 1992; Yamagishi et al., 1992). In guinea-pig coronory myocytes, membrane voltage has been shown to modulate IP_3 synthesis in a bipolar manner (Ganitkevich and Isenberg, 1993). In rat megakaryocytes, (a nonexcitable cell), membrane potential has also been shown to play an important role in calcium oscillations by modulating IP_3 synthesis in a bipolar manner (Mahaut-Smith et al., 1999; Mason et al., 2000; Mason and Mahaut-Smith, 2001). Membrane potential is also reported to modulate IP_3 receptor-modulated Ca^{2+} release in skeletal muscle (Donaldson et al., 1988; Vergara et al., 1985). In guinea-pig stomach smooth muscle, IP_3 receptor-modulated Ca^{2+} release (Suzuki and Hirst, 1999; van Helden et al., 2000), and the frequency of slow waves are dependent on membrane potential (Huang et al., 1999; Nose et al., 2000; van Helden et al., 2000). All these studies establish a role for membrane potential in regulation of Ca^{2+} release and oscillations through a feedback on IP_3 synthesis.

In a previous study (van Helden et al., 2000), we examined the role of membrane potential in generation and control of slow waves in guinea-pig pyloric smooth muscle. Now we further investigate the role of voltage feedback on IP_3 synthesis and its effect on slow waves using a parsimonious, qualitative mathematical model that includes known relationships between key variables. Our model incorporates Ca^{2+} release from intracellular stores, resultant inward current(s), and voltage feedback on IP_3 synthesis. It is important to note that our model only considers the case where voltage-dependent channels (e.g. L-Ca^{2+} channels) are blocked, as the voltage feedback on IP_3 synthesis is known to occur independent of L-Ca^{2+} channels (Suzuki and Hirst, 1999; van Helden et al., 2000).

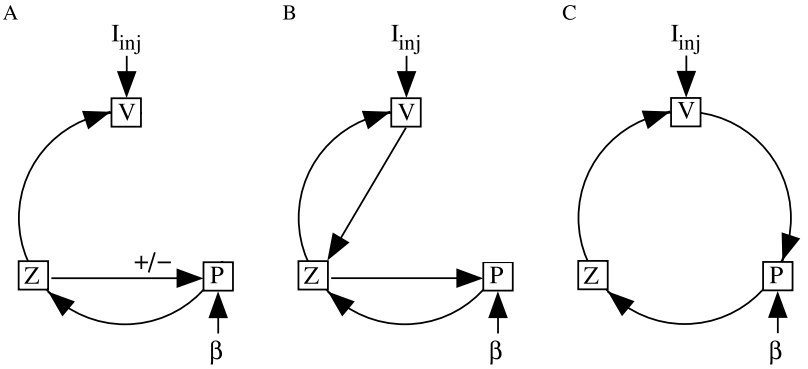

FIGURE 1 Feedback loops for IP_3 synthesis. (*A*) Ca^{2+} (*Z*) can modulate IP_3 (*P*) through either a positive or negative feedback loop. (*B*) Membrane voltage (*V*) modulates IP_3 indirectly through Ca^{2+}. (*C*) Membrane voltage feedback on IP_3 synthesis. All arrows denote positive interaction except where noted. I_{inj} is current injected into the cell, and β is the external stimulus.

Many mathematical models have been proposed to study calcium oscillations. Some of these models describe calcium oscillations assuming nonoscillating IP_3 (Dupont et al., 1990; Dupont and Goldbeter, 1993; Hofer, 1999), whereas others have incorporated IP_3 oscillations in the model. The latter models have used the finding that there is a feedback of Ca^{2+} on IP_3 synthesis, see Fig. 1 *A*, thereby inducing IP_3 oscillations. This feedback of Ca^{2+} on IP_3 synthesis can be either positive (De Young and Keizer, 1992; Keizer and De Young, 1993; Meyer and Stryer, 1991), or negative (Dupont and Erneux, 1997; Houart et al., 1999). Keizer and De Young (1993) included an indirect effect of membrane voltage on IP_3 synthesis by combining voltage-activated calcium influx and positive feedback of Ca^{2+} on IP_3 synthesis. In this model (Keizer and De Young, 1993), membrane voltage activates calcium influx into the cytosol and calcium in the cytosol in turn increases IP_3 synthesis through a positive feedback loop, Fig. 1 *B*.

In the present study we examine Ca^{2+} oscillations where membrane voltage exerts a positive feedback on IP_3 synthesis, as shown in Fig. 1 *C*. We do not consider the effects of voltage-activated influx of Ca^{2+} in our model, as our observations are based on experiments where voltage-gated channels have been blocked (see Methods in van Helden et al., 2000). We use a single pool model (Dupont and Goldbeter, 1993) as a basic model that captures the calcium dynamics of our system. We extend this model (Dupont and Goldbeter, 1993) by including membrane potential and its interaction with intracellular IP_3.

In the remainder of this paper we begin by summarizing the experimental results of our previous work (van Helden et al., 2000). Experiments are divided into two sets. The first set involves injection of maintained current into the tissue, whereas the second set involves injection of current pulses. Based on these experimental results, we then formulate a mathematical model and describe the general properties of this model.

Our model shows that an oscillatory region exists for membrane potential and external stimulus (such as application of an agonist known to increase IP_3) in a two parameter bifurcation plot. Slow wave frequency varies if the stimulus is held constant while membrane potential is changed. Moreover, slow waves can be induced or abolished by a combination of stimuli and membrane potential. This model behavior is consistent with experimental observations.

Next we show that voltage pulses can evoke a response due to excitability near the Hopf Bifurcation point. Membrane potential can evoke excitable responses indirectly by changing IP_3 concentration in the cytosol ($[IP_3]_c$). It is shown that the sequence of events following hyperpolarizing and depolarizing pulses is different. The difference in latency of responses to these protocols is investigated in detail. It is shown that a minimum interpulse duration is required to evoke a full response from the tissue. This minimum interpulse duration is shown to vary with the steady-state level of the stimulus and holding potential. These results are also consistent with experimental observations. We conclude by considering the biological significance of the postulated mechanisms.

We note that the bifurcation analysis was carried out using AUTO (Doedel and Kernevez, 1986) included in the numerical package XPPAUT (Ermentrout, 1994). Numerical simulation and analysis were performed using MATLAB (Mathworks Inc. Natick, MA) and XPPAUT.

EXPERIMENTAL RESULTS

We base our model on observations made from intracellular recordings of membrane potential in electrically short strips of guinea-pig gastric pylorus smooth muscle. These observations have been described in our previous work (van Helden et al., 2000). The experiments can be divided into two sets.

Experiment set 1: maintained current injection

The first set involves injecting maintained current into the tissue and monitoring the tissue response. This procedure was repeated alone and in combination with different concentrations of an agonist (acetylcholine (ACh)) known to increase IP_3.

Observations from these experiments can be summarized as follows. 1.1) Slow wave frequency increased when resting membrane potential was held at a depolarized level and decreased when tissue preparations were hyperpolarized. 1.2) The peak depolarization attained by the slow wave was weakly dependent on holding potential. 1.3) Slow waves could often be induced in quiescent tissues by membrane depolarization. 1.4) Slow waves could be abolished by large hyperpolarization. 1.5) The decrease in slow wave frequency caused by hyperpolarization could be counteracted by addition of agonists that induce synthesis of IP_3, (e.g., ACh).

Experiment set 2: pulsed current injection

The second set of experiments involved injecting pulses of current to induce step changes in membrane potential. This procedure was carried out separately and in combination with the first set of experimental protocols.

Observations from these experiments can be summarized as follows. 2.1) A single current pulse of appropriate size occasionally evoked a train of slow waves in a previously quiescent tissue. 2.2) Current pulses induced either a subthreshold response or a full slow wave response. 2.3) A current pulse that induced a full slow wave response required a minimum amplitude and duration. 2.4) Holding the membrane potential at a hyperpolarized level decreased the probability of evoking a full slow wave response with a current pulse, whereas the opposite applied for depolarization. 2.5) The latency of the response (defined here as the time lag between the rising edge of the stimulating current pulse to the peak of the evoked response) was reduced with increasing pulse strength (absolute pulse amplitude) and approached a minimum value that could not be reduced with increasing pulse strength. 2.6) Increasing the agonist concentration reduced the latency of response. 2.7) The minimum latency of response to a hyperpolarizing pulse was longer than for a depolarizing pulse. 2.8) A minimum interpulse duration between applied voltage pulses was required to evoke a full slow wave response.

Our purpose here is to construct a mathematical model displaying these experimentally observed properties.

MODEL

We simplify our system by considering the case of a single isopotential cell with a single IP_3 receptor operated intracellular calcium pool. Ryanodine receptors do not play a major role in generation of slow waves as slow waves persist even when ryanodine receptors are blocked (van Helden et al., 2000). Thus, we have ignored rynodine receptors in our model.

Calcium dynamics

We follow the original notation of the single pool model of Dupont and Goldbeter (1993) for Ca^{2+} concentrations in the cytosol ($[Ca^{2+}]_c$) and IP_3-sensitive intracellular Ca^{2+} store ($[Ca^{2+}]_s$) and denote them by the state variables Z and Y, respectively. We denote IP_3 concentration in the cytosol ($[IP_3]_c$) by the state variable P. The coupled ordinary differential equations describing the Ca^{2+} dynamics are:

$$\frac{dZ}{dt} = V_{in} - V_2 + V_3 + k_f Y - KZ \tag{1}$$

$$\frac{dY}{dt} = V_2 - V_3 - k_f Y \tag{2}$$

$$V_{in} = V_0 + V_1 P \tag{3}$$

$$V_2 = V_{M2} \frac{Z^n}{k_2^n + Z^n} \tag{4}$$

$$V_3 = V_{M3} \frac{Z^w}{k_a^w + Z^w} \frac{Y^m}{k_r^m + Y^m} \frac{P^0}{k_p^0 + P^0} \tag{5}$$

in which V_{in} is the Ca^{2+} influx from extracellular space (composed of an IP_3 independent component (V_0) and an IP_3 dependent component (V_1P)). Ca^{2+} is expelled from the cytosol into the extracellular space by a $[Ca^{2+}]_c$ dependent pump, represented by the term KZ. V_2 is the Ca^{2+} flux into the intracellular Ca^{2+} store. V_3 is the Ca^{2+} and IP_3 dependent release of calcium from the intracellular Ca^{2+} store. The term k_fY represents the leakage from the store dependent on the $[Ca^{2+}]_s$. Parameters for the system defined by Eqs. 1 to 5 are summarized in Table 1.

Membrane current and potential

Ca^{2+} oscillations in the cytosol result in the slow wave depolarizations. Ca^{2+}-voltage coupling is brought about by a Ca^{2+}-modulated current through a nonselective cationic channel. Ca^{2+}-modulated conductance, G_{ca}, for this channel is defined by the following equation:

$$G_{ca} = G_{Mca} \frac{Z^q}{k_{ca}^q + Z^q} \tag{6}$$

in which G_{Mca} is the maximum value for this conductance and k_{ca} is the half saturation constant for G_{Ca}.

We add to the basic model (Eqs. 1–5) a new state variable V, the membrane potential of the cell. The current and voltage dynamics, including the Ca^{2+}-modulated current, is described by:

$$C_m \frac{dV}{dt} = G_i(V - E_i) - G_{ca}(V - E_{ca}) + I_{inj} \tag{7}$$

in which C_m is the capacitance of the membrane. A "lumped current" passing through passive ionic channels is repre-

TABLE 1 Parameters related to Ca^{2+} dynamics given by Eqs. 1 to 5

	Parameter descriptin	Value
V_0	Constant Ca^{2+} influx from extracellular space into cytosol	3.4 μM/min
V_1	IP_3 dependent Ca^{2+} influx from extracellular space into cytosol	3.4 μM/min
k_f	Rate constant for Ca^{2+} leak from store to cytosol	1 min^{-1}
K	Rate constant for Ca^{2+} extrusion from the cytosol	10 min^{-1}
V_{M2}	Maximal value for Ca^{2+} pump into the store	50 μM/min
n	Hill coefficient	2
k_2	Cytosolic Ca^{2+} dependent threshold constant for V_2	1 μM
V_{M3}	Maximal value for Ca^{2+} release from the store	650 μM/min
w	Hill coefficient	4
k_a	Cytosolic Ca^{2+} dependent threshold constant for V_3	0.9 μM
k_r	Store Ca^{2+} dependent threshold constant for V_3	2 μM
m	Hill coefficient	2
k_p	IP_3 dependent threshold constant for V_3	0.65 μM
o	Hill coefficient	4

sented by the first right hand side term. The second term gives the Ca^{2+}-modulated current, whereas I_{inj} is the current injected into the cell to control the membrane potential. Voltage-gated channels are not considered (these were blocked in all experiments). Thus, all conductances in Eq. 7, except G_{Ca}, are taken as constant. A summary of parameters for the system defined by Eqs. 6 and 7 is given in Table 2.

IP_3 dynamics

Membrane potential has a positive feedback on IP_3 synthesis (van Helden et al., 2000). We include this membrane potential dependent synthesis of IP_3 by defining a function $P(V)$. It was noted in the experimental observations above that polarizing the membrane is effective in modulating tissue response only within a given range of values. This observation suggests that the function $P(V)$ has a sigmoidal response to V. Taking this observation into account we define $P(V)$ as follows:

$$P(V) = P_{MV}\left(1 - \frac{V^{\tau}}{k_V^{r} + V^{\tau}}\right) \tag{8}$$

in which P_{MV} is the maximal rate of voltage dependent IP_3 synthesis. The parameter k_V is the membrane potential at half value of the $P(V)$ curve (see Fig. 4 *C*), and it determines the voltage dependent IP_3 synthesis at resting membrane potential. It was noted in the experimental observations above that hyperpolarizing the tissue from its resting potential decreases the slow wave frequency, which suggests that at resting membrane potential $P(V)$ contributes significantly to the total $[IP_3]_c$. The parameter k_v has been chosen to take this observation into account. k_v was further adjusted to match the experimentally observed slow wave frequency response to changes in resting membrane potential (see figure 6 in van Helden et al., 2000).

Now we include the function $P(V)$ in the overall IP_3 dynamics so that membrane potential exerts a positive feedback on IP_3 synthesis (Fig. 1 *C*). We use a formulation similar to (Houart et al., 1999) to describe the IP_3 dynamics in the cell, that is,

$$\frac{dP}{dt} = \beta - \varepsilon P - V_{M4}\frac{P^{u}}{k_4^{u} + P^{u}} + P(V) \tag{9}$$

IP_3 can be modulated by external stimuli (such as application of ACh), denoted by the term β. Both linear and nonlinear mechanisms degrade IP_3, as described by the second and third terms. The fourth term describes the dependence of IP_3 on voltage (i.e., Eq. 8).

It is known that there is a Ca^{2+} -stimulated degradation of IP_3 (Berridge, 1993b; Houart et al., 1999; Takazawa et al., 1990). Although we have not included this kinetic effect on IP_3 dynamics explicitly, our use of experimental data accounts for it implicitly. We leave a more detailed biochemical model for future work. Table 3 summarizes the parameters for the IP_3 system used in Eqs. 8 and 9.

Eq. 1–9 constitute a simplified mathematical model based on the experimental observations given above. This system will be referred to hereafter as the "model cell." Physiological experiments carried out on the tissue are repeated using numerical simulations on the model cell to study the feedback of voltage on IP_3 synthesis and its role in Ca^{2+} release and slow wave regulation.

TABLE 2 Parameters related to membrane voltage and currents given by Eqs. 6 and 7

	Parameter description	Value
C_m	Membrane capacitance	0.0017 F
G_i	Lumped conductance of passive ionic channels	1.12 mS
E_i	Lumped reversal/null potential of passive ionic channels	−67.2 mV
E_{ca}	Reversal/null potential for the Ca^{2+} modulated current(s)	−20 mV
G_{Mca}	Maximal value of G_{ca}	4 mS
k_{ca}	Half saturation constant for G_{Ca}	1.4 μM
q	Hill coefficient	4

RESULTS

Calcium, membrane potential, and IP_3 dynamics

Ca^{2+} increases in the cytosol result in membrane depolarization, Fig. 2 *A*. However, due to the nonlinear property of

TABLE 3 Parameters related to IP_3 dynamics given by Eqs. 8 and 9

	Parameter description	Value
P_{MV}	Maximal rate of voltage dependent IP_3 synthesis	0.8 μM/min
k_v	Half saturation constant for voltage dependent IP_3 synthesis	−58 mV
r	Hill coefficient	8
β	External stimulus generated IP_3	0.7 μM
ε	Rate constant for linear IP_3 degradation	0.9 min^{-1}
V_{M4}	Maximal value for the nonlinear IP_3 degradation	2 μM/min
k_4	Half saturation constant for the nonlinear IP_3 degradation	0.5 μM
u	Hill coefficient	4

the Ca^{2+} -activated conductance, G_{ca}, only Ca^{2+} above a certain threshold is effective in causing depolarizations. This is apparent in Fig. 2 *A*, where Ca^{2+} changes result in voltage modulation, except near the baseline. A constant external stimulus (β) results in a steady level of $[IP_3]_c$. An oscillatory $[IP_3]_c$ component is added to this steady level due to the voltage modulated IP_3 synthesis. However, because membrane voltage modulates only the *rate* of IP_3 synthesis, changes in voltage are followed by changes in $[IP_3]_c$ with a lag. Ca^{2+} facilitates further Ca^{2+} release through this new pathway, Eq. 8, as well as CICR governed by Eq. 5.

This calcium system can be externally controlled by application of agonist (effectively changing the magnitude of β and hence IP_3 synthesis) and/or by means of current injection (I_{inj}) (effectively changing membrane voltage). The calcium system is more sensitive to voltage changes given the larger Hill coefficient of the voltage activated IP_3 synthesis (parameter r in Eq. 8). However, the maximum value of voltage activated synthesis of IP_3 (P_{MV}) is small compared with the maximum range of β variation, therefore β is more effective in changing the system. The combined effect of external stimulus and membrane voltage is denoted by $F(\beta, V)$. The nullclines of the state variables Z and Y are shown in Fig. 2 B. The curve SS′ shows the path traveled by the steady-state S_o as V and/or β are changed. The thick section shown on SS′ denotes the region where the system is oscillatory. The location of steady-state S_o is dependent on the function $F(\beta,V)$. The shapes of the nullclines are similar to those obtained with the single pool model (Dupont and Goldbeter, 1993). However, with the added voltage feedback, any change in membrane potential results in a change of the nullclines due to voltage dependent IP_3 changes. Thus, even when β is constant, nullclines will constantly change shape due to voltage oscillations.

A single parameter bifurcation diagram of Ca^{2+} with respect to stimulus β is shown in Fig. 2 *D*. Oscillations arise through a subcritical Hopf bifurcation with a hard-loss of stability (Edelstein-Keshet, 1988). The frequency of oscillations increases with increasing β, Fig. 2 *C*. The system is bistable over a range of β values ($\beta_0 < \beta < \beta_h$), as shown in the inset of Fig. 2 *D*. In this bistable range, a stable nonperiodic steady state co-exists with stable and unstable periodic orbits, Fig. 3 *B*. The stable steady state is sur-

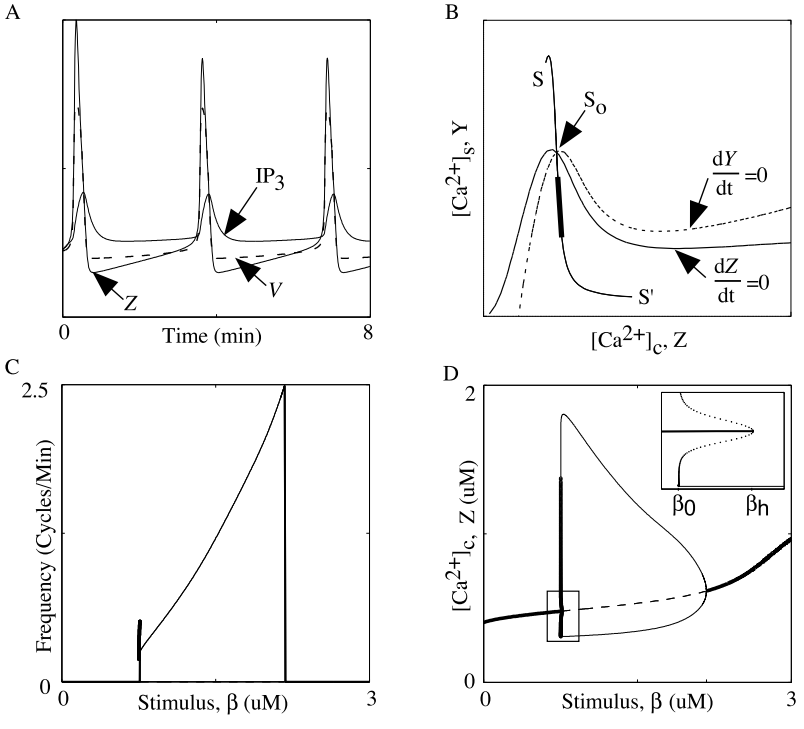

FIGURE 2 Dynamics of the voltage-dependent system. (*A*) Intracellular Ca^{2+} (Z) and membrane potential (V) oscillations are in phase, whereas IP_3 oscillations follow with a lag. All traces are normalized. (*B*) Schematic nullclines $dZ/dt = 0$ and $dY/dt = 0$. Path of steady state as a function of $F(\beta, V)$ given by line SS', thick part of the line represents stable oscillations. S_0 is the instantaneous steady state of the system. The ends of the thick solid line represent the two Hopf points. (*C*) Frequency of oscillation plotted against stimulus β. (*D*) Bifurcation diagram for Ca^{2+} with β as the parameter. Oscillations arise and end through the two Hopf bifurcation points. Inset shows the bistable region, $\beta_0 < \beta < \beta_h$, (in box) enlarged. Stable steady states (*thick solid*); unstable steady states (*dashed*); maxima and minima of stable oscillations (*solid*); and unstable oscillations (*dots*). $\beta = 0.8$ μM and $I_{inj} = 0$ mA for part *A* of this figure, remaining parameter values for this and all subsequent figures are given in Tables 1 to 3. Typical initial conditions $Z = 0.475$ μM, $Y = 4.439$ μM, $V = -65.09$ mV, $P = 0.397$ μM.

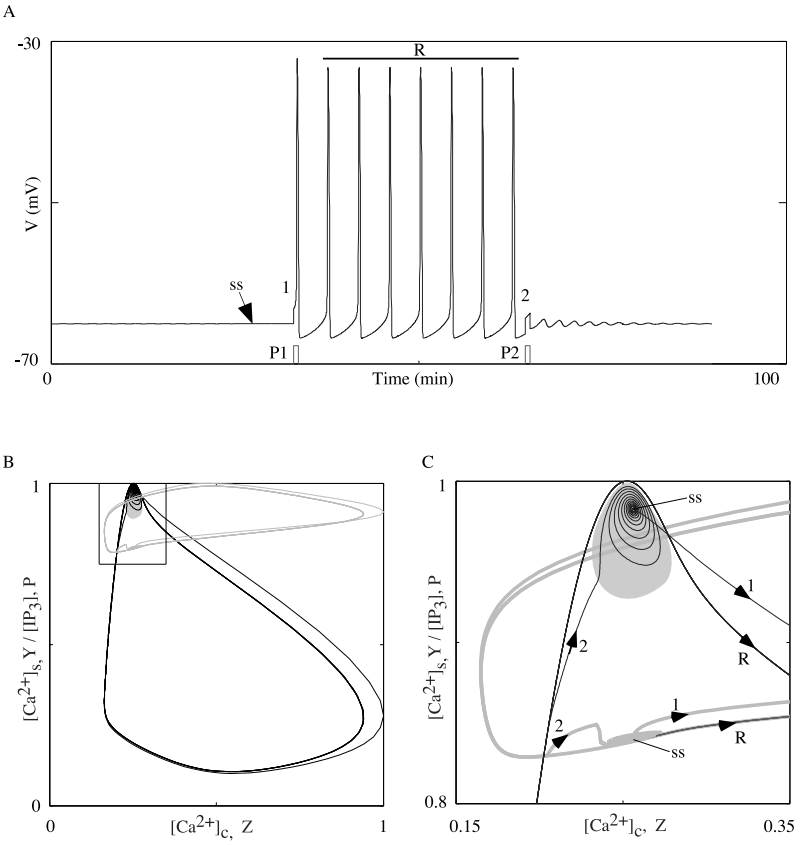

FIGURE 3 Pulse evoked/abolished slow wave train in the bistable region. (*A*) In the bistable region (Fig. 2 *D*), a current pulse of appropriate amplitude and duration can induce slow wave train in a previously inactive cell. The first pulse P1 pushes the trajectory into stable oscillations while the second pulse P2 pushes it back into the region of unstable periodic orbits (basin of attraction), where it eventually settles down to the stable nonperiodic steady state. Voltage pulses labeled 1 and 2 result from the current pulses P1 and P2 (2.25 mA). Slow waves labeled *R* indicate repetitive oscillations. Label *ss* indicates the nonperiodic steady state. (*B*) Trace given in *A* is now shown in the normalized *Z*-(*Y*,*A*) plane. Shaded region shows approximately the basin of attraction of the nonperiodic steady state *ss*. (*C*) Enlarged view of boxed region in *B*. Numbered arrows refer to the events on the rising edge of the pulses (see injected pulses in *A*). Note that direction of *Z*-*Y* and *Z*-*A* trajectories are opposed. Thick lines are IP_3, and solid lines Ca^{2+} trajectories. Parameter values are the same as for Fig. 2, except $\beta = 0.755$ μM.

rounded by a region of unstable periodic orbits (shaded region in Fig. 3 *B*), forming a "basin of attraction." Current pulses of sufficient amplitude and duration can push the trajectory in or out of the basin of attraction and thus inducing or abolishing slow wave train, as shown in Fig. 3 *A* and *C*. Although this model behavior accords with our experimental observation 2.1, no significant biological conclusions can be drawn due to the narrow range of bistability (inset in Fig. 2 *D*), where this behavior is possible.

Slow wave voltage dependence

The first set of experiments (maintained current injection) investigated the role of membrane potential by holding the resting membrane potential and β at various predetermined levels. These experiments were simulated using the model cell. In the model cell, slow waves were observed to persist only within specific bounds of stimuli and holding potential. At any constant β, the frequency of slow waves displayed a significant dependence on holding potential, whereas peak depolarizations reached by the slow waves were weakly dependent on holding potential (Fig. 4 *A*). Hyperpolarizations decreased the frequency of the slow waves whereas the opposite was true for depolarizations (Fig. 4 *B*). These results from the model are consistent with experimental observations 1.1 and 1.2.

It was stated earlier that the steady state, S_o, is dependent on the function $F(\beta,V)$. This is explored numerically with two parameter bifurcation diagrams shown in Fig. 5. A single parameter (β) bifurcation diagram was shown previously (Fig. 2 *D*). Now we want to study bifurcation with respect to β and voltage (via I_{inj}). To achieve this, we plot the bifurcation diagram of Fig. 2 *D* for different values of I_{inj}, as shown in Fig. 5 *A*. It can be seen from Fig. 5 *A* that as I_{inj} is changed, the oscillatory region shifts on the β axis. This three-dimensional figure is projected on the β and I_{inj} plane for clarity and shown as Fig. 5 *B*. The system is oscillatory for combinations of β and I_{inj} within the shaded region O. The single parameter bifurcation diagram given in Fig. 2 *D* is a vertical section on the line $I_{inj} = 0$ in Fig. 5 *A*. The two Hopf points HP_1 and HP_2 for $I_{inj} = 0$ are shown as solid squares. As I_{inj} is changed, the two Hopf points trace the edges of the shaded region O.

The shape of the region O is primarily defined by Eq. 8. While the system is in a nonperiodic steady state ($\beta < \beta_2$ and $I_{inj} = 0$), a constant contribution is made by $P(V)$ to the $[IP_3]_c$ (Fig 4 *C*). The existence of this contribution is evident from the observation that hyperpolarizing the tissue reduces the frequency of oscillation (an indication that IP_3 has been reduced).

Voltage polarizations influence the frequency of the slow waves only within a specific range. The limits of this range

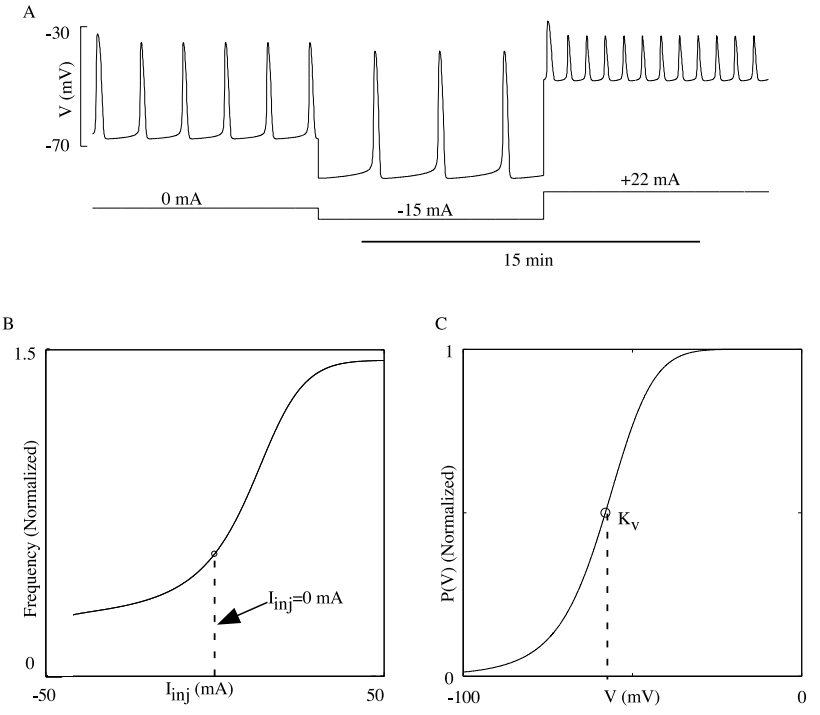

FIGURE 4 Slow wave voltage dependence. Effects on slow waves oscillations of polarizing the membrane potential to different voltage levels. (*A*) Membrane potential was polarized by injecting 0, −15, and +22 mA current into the cell. Hyperpolarization (depolarization) of the tissue reduced (increased) the frequency of oscillations. (*B*) Frequency of slow waves as a function of I_{inj}. (*C*) Dependence of IP_3 synthesis on membrane potential. K_V is membrane potential at half P_{MV}.

are defined by the Hill coefficient r and approximately indicated by lines MM′ and NN′ in Fig. 5 *B*. Increasing r causes this limit to decrease (i.e., lines MM′ and NN′ move closer together because the slope of $P(V)$, (Fig. 4 *C*), becomes steeper). Increasing P_{MV} moves the region O to the left, increasing sensitivity of the system to external stimuli, whereas decreasing P_{MV} moves it to the right, decreasing sensitivity to external stimuli. Setting $P_{MV} = 0$ collapses the lines MM′ and NN′ onto the line $I_{inj} = 0$; the edges of region O becomes straight and no longer intersect the line $I_{inj} = 0$ at β_2 (HP_1) and β_5 (HP_2). In this case, the membrane potential decouples from IP_3 synthesis and the system is reduced to the single pool model (Dupont and Goldbeter, 1993). Now, $P_{MV} = 0$, voltage changes (or I_{inj} changes) have no effect on Ca^{2+} dynamics and oscillations arise through the original Hopf bifurcation points (now dependent on β only), which lie to the right of HP_1 and HP_2.

It was stated in the first set of observations (experimental observations 1.3) that slow waves could be induced in an inactive (nonoscillatory) tissue by depolarizing the membrane. This behavior is indicated in Fig. 5 *B* by the arrows. Any nonoscillatory state of the system β_{12} (where $\beta_1 < \beta_{12} < \beta_2$) can be moved into the oscillatory region, by polarizing the membrane potential to a sufficiently elevated voltage. Similarly, an oscillating system located on point β_{23} (where $\beta_2 < \beta_{23} < \beta_3$), slow waves can be abolished by sufficiently hyperpolarizing the membrane, consistent with experimental observation 1.4. This phenomena is dependent on the shape of the region O, which is dependent on the parameter r (as discussed above). It is interesting to note that similar results would be expected on the other edge of the bounded region O but with reversed polarities of I_{inj} (see large arrows in Fig. 5 *B*). In addition, starting at any point in the bifurcation space of β and I_{inj}, it is possible to maintain a constant oscillation frequency by traveling parallel to the edges of the region O, thereby defining a set of isofrequency lines. This model behavior is in accordance with experimental observation 1.5.

In summary, the simulations of slow wave voltage dependence using the model cell accord with the observations made during experiments with maintained current injection (experiment set 1).

Voltage evoked response

The second set of experiments investigated tissue responses to injected current pulses. These experiments were simulated using the model cell by injecting current pulses to induce step changes in membrane potential. Two types of responses of the model cell to these pulses were observed, a large full slow wave, and a smaller subthreshold response (Fig. 6 *A* and *B*). These responses are consistent with experimental observation 2.2. We will begin by describing the full slow wave response.

Injected current pulses were able to evoke slow wave responses only if they could induce a voltage change that was above a critical amplitude (ΔV_c) and duration (t_c). Reducing β moved the steady state of the system further from the Hopf point HP_1, Fig. 2 *B*, and so required a larger ΔV_c to evoke full slow wave responses. A subthreshold pulse of long duration was insufficient to produce a slow

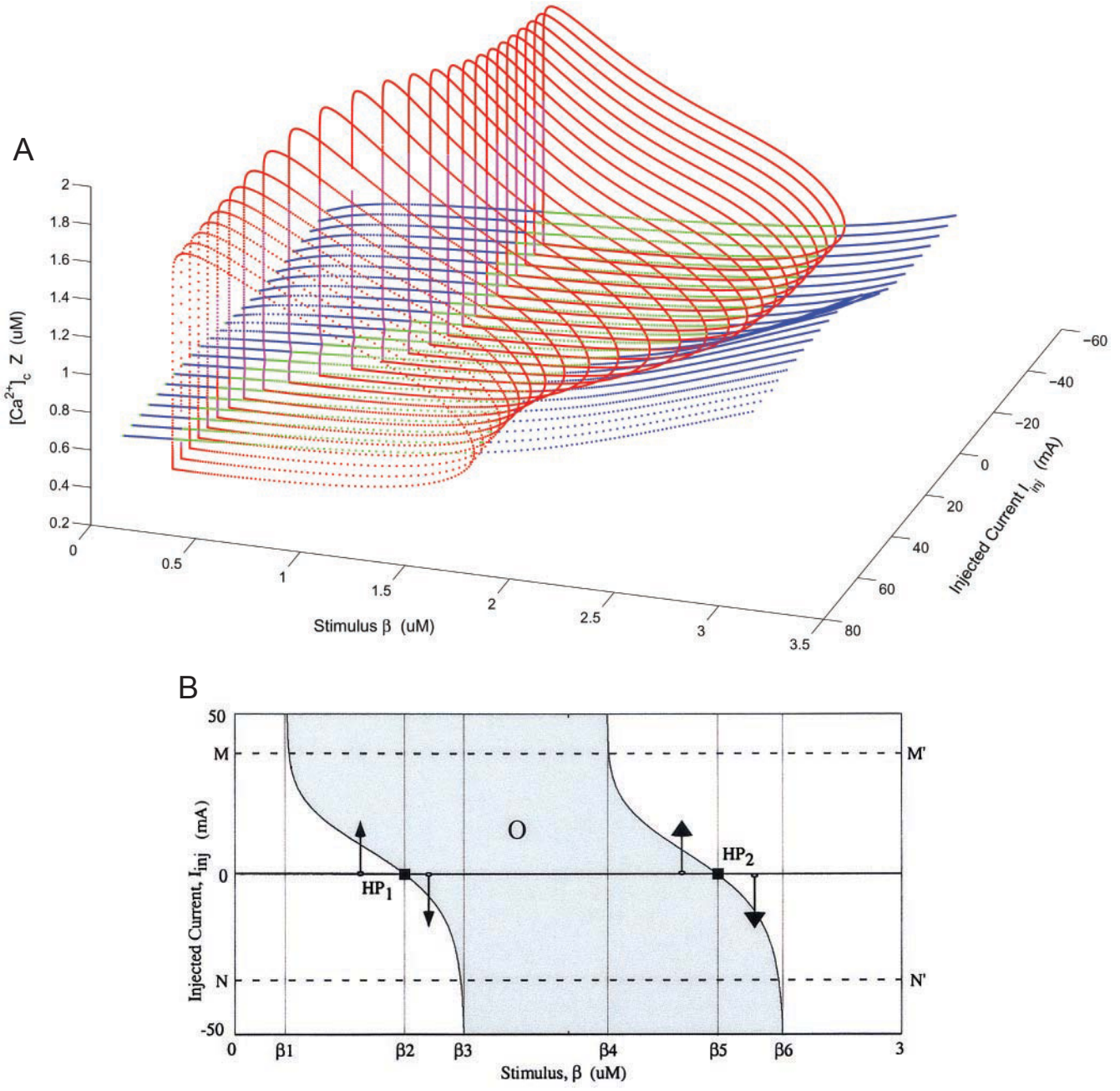

FIGURE 5 Two parameter (I_{inj} and β) stability diagram for Ca^{2+} oscillations. (*A*) Oscillatory region changes location on the β axis as I_{inj} is varied. The single parameter (β) bifurcation diagram given in Fig. 2 *D* is a vertical section of this three-dimensional volume on the line $I_{inj} = 0$. Stable steady states (*blue*); unstable steady states (*green*); maxima and minima of stable oscillations (*red*); and unstable oscillations (*magenta*). (*B*) The bifurcation diagram in part *A* projected on the β-I_{inj} plane. See text for details.

wave response. If a full slow wave response was generated, it was always initiated at the rising edge of the pulse.

The preceding model behavior is consistent with and provides an explanation for the experimental observation 2.3. We can now also explain observation 2.4 (changing the resting membrane potential influenced the probability of evoking a response from the tissue). Because the steady state of the system is controlled by the function $F(\beta,V)$, changing the membrane potential will change the excitability of the system (see below for further details). Thus, depolarizing the membrane would increase (and hyperpolarizing the membrane would decrease) the excitability of the tissue. This, in turn would increase (and decrease, respectively) the probability of evoking a slow wave response to a voltage pulse, consistent with observation 2.4. Furthermore, based on this argument, the model also predicts that

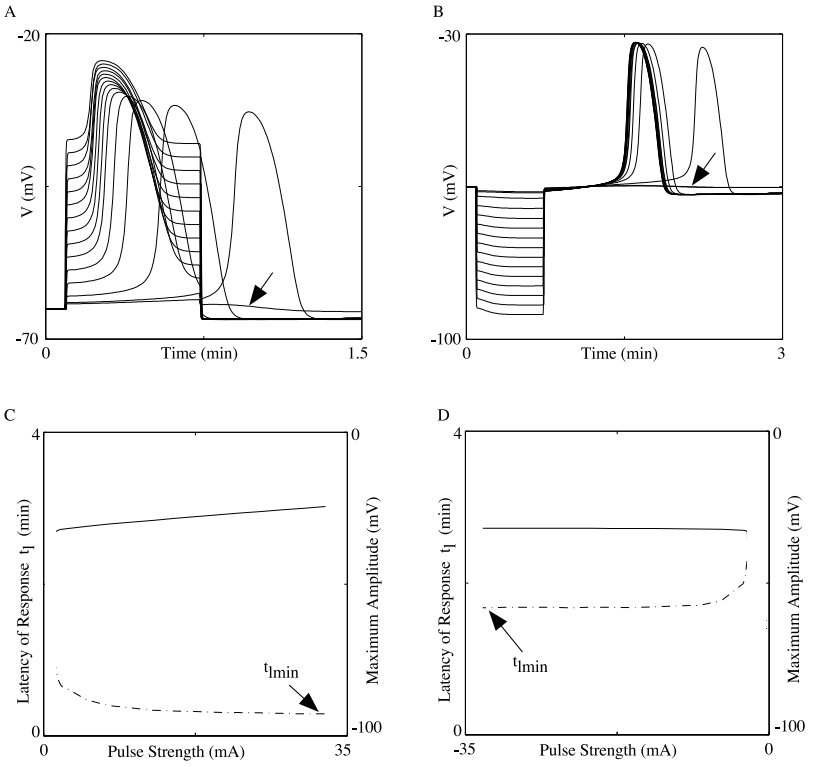

FIGURE 6 Latencies and amplitudes of pulse-induced responses. The responses and voltage dependence of the latencies to depolarizing (*A* and *C*) and hyperpolarizing (*B* and *D*) current injections. Examples of responses to depolarizing (*A*) and hyperpolarizing (*B*) pulses. Arrows denote subthreshold responses. The latencies of the responses decreased with absolute pulse amplitudes and approached minimum values, dashed-dot lines in *C* and *D*. Note the larger minimum latency in case of hyperpolarizing pulses. Pulse-induced slow wave amplitudes increased with pulse strength for depolarizing pulses while they remained constant in response to hyperpolarizing pulses, solid lines in *C* and *D*, respectively. Parameter values same as Fig. 2 except $\beta = 0.7\ \mu$M.

minimum pulse amplitude required to evoke a response from the tissue would also depend on the agonist level.

The latency of a slow wave response (t_1) is defined here as the time lag between the rising edge of the stimulating current pulse and the peak of the evoked response. t_1 was found to vary inversely with the absolute amplitude of the stimulating pulse (pulse strength) (Fig. 6). However, t_1 could not be reduced indefinitely by increasing the pulse strength. It approached a minimum value ($t_{1\min}$), and increasing the pulse strength beyond a certain level had no further effect. This model behavior is consistent with experimental observation 2.5. As discussed in the preceding paragraph, changing agonist concentration would increase the excitability of the system, thus reducing the latency of response. This is also consistent with observation 2.6.

The latency curves, (Fig. 6, *C* and *D*) were markedly different for depolarizing and hyperpolarizing pulses. Responses to hyperpolarizing pulses showed longer latencies and also a longer minimum latency $t_{1\min}$. The peak amplitude of the hyperpolarization-induced slow wave was always of the same magnitude, Fig. 6, *B* and *D*, whereas the peak amplitude for the depolarization-induced slow wave was found to increase slightly with increasing pulse strength, Fig. 6, *A* and *C*.

Phase plane analysis was used to investigate the details of the pulse-induced responses. The nullclines are of a shape commonly referred to as "S" or "N", (Fig. 2 *B*). This nullcline shape is typical for excitable systems (Edelstein-Keshet, 1988; Sneyd et al., 1993), such as the FitzHugh-Nagumo model of the nerve axon (FitzHugh, 1961; Nagumo et al., 1964), and so a similar analysis can be applied to our system.

Properties of the pulse-induced response become evident by examining the evolution of the system in the phase plane. As the two parameters, β and I_{inj} (external stimulus and injected current) are changed, the steady state of the system moves through the phase plane on the path SS', as shown in Fig. 2 *B*. A positive change in either the membrane potential (via current injection I_{inj}), or agonist concentration (β), or both, moves the steady-state S_0 downward towards S'. Negative changes in these two parameters raise the steady state towards S.

If the system is on a nonperiodic steady state (shown as S_0 in Fig. 7), a basin of attraction exists near S_0 (Fig. 3 *B*). Any initial condition starting within this basin settles down to S_0 with small decreasing oscillations. However, if the initial condition lies outside this region, a large excursion is executed before the system returns to S_0.

Let the existing state of the system be S_0. A current pulse of duration t_p is applied, which induces a step change in voltage, ΔV. Upon application of the pulse, a new steady-state $\bar{S}$ is created instantaneously. Let the instantaneous state of the system be given by S^*. S^* moves from S_0 to the new steady-state $\bar{S}$ in time $\bar{t}$.

In the case of a hyperpolarizing pulse, Fig. 7 *A*, the pulse would induce a negative change in voltage and $\bar{S}$ would lie above S_0. The following can now happen. If $t_p < \bar{t}$, the pulse would terminate before S^* reaches $\bar{S}$. Because the pulse has

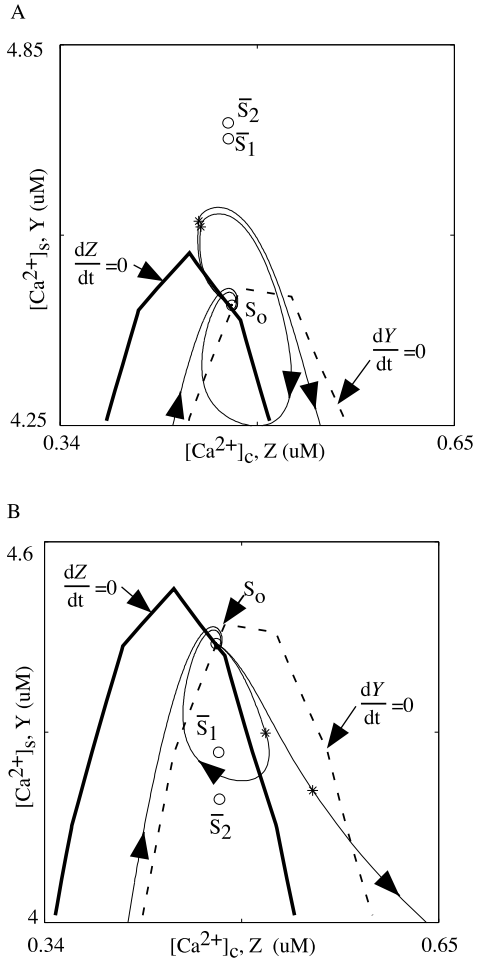

FIGURE 7 Sub- and super-threshold responses to hyperpolarizing (*A*) and depolarizing (*B*) pulses. Thick solid lines are the $dZ/dt = 0$ nullclines and dashed lines are $dY/dt = 0$ nullclines. S_0 is the initial steady state. Immediately after the initiation of the pulse, $\bar{S}_1$ are the subthreshold and $\bar{S}_2$ the superthreshold steady states. A hyperpolarizing (depolarizing) pulse moves the steady state upward (downward) on the line SS' (Fig. 2 *B*). Asterisks denote the position of the instantaneous states of the system S^* at the time of termination of the pulse (t_p). Note that the full slow wave is not shown in its entirety, only the initial and final parts are included. Parameter values are the same as for Fig. 2, except $\beta = 0.7$ μM.

terminated, $\bar{S}$ has instantaneously jumped back to S_0. As S^* tries to return to S_0, two things can happen: 1) if the pulse is of sufficient duration ($t_p > t_c$) and sufficient amplitude (to cause $\Delta V > \Delta V_c$), then S^* can escape the basin of attraction of S_0 (Fig. 3 *B*). S^* will make a large detour before settling down to S_0, and this would be a pulse-induced full slow wave response; 2) if the pulse has terminated too quickly ($t_p < t_c$) or the pulse was not strong enough ($\Delta V < \Delta V_c$), then S^* is too close to S_0 and it will not escape the basin of attraction of S_0. Instead, S^* will settle down to S_0 quickly and this will be a subthreshold response.

If $t_p > \bar{t}$, S^* would reach $\bar{S}$ and new dynamics will ensue as described in the previous section.

If the current injection is positive, Fig. 7 *B*, the new steady state will be below S_0 and S^* will travel first to the right, settling to $\bar{S}$ in time $\bar{t}$. Full slow wave or subthreshold response events would be induced in the same way as described for the hyperpolarizing pulse.

An important difference between the responses to pulses of different polarities is the initial direction that S^* travels in the phase space upon injection of the pulse. For hyperpolarizing pulses, the initial direction that S^* travels is to the left and upward; this direction of travel is in fact opposite to the direction S^* must travel before reaching its final state. Hence, upon termination of the hyperpolarizing pulse, S^* must retrace the horizontal distance to the right before settling down to S_0, the state at the end of the response. On the other hand, the initial direction that S^* travels in response to a depolarizing pulse is to the right and downward, which is the direction S^* must travel to arrive at its final state S_0 at the end of the response. Thus, the latency of response from hyperpolarizing pulses must include the retracing component and is larger compared with the latencies from depolarizing pulses. This would explain why the latencies observed following hyperpolarizing pulses are larger than those seen following depolarizing pulses (Fig. 6 *C* and *D* and experimental observations 2.7).

Effect of interpulse duration

The effect of interpulse duration (experimental observation 2.8) was studied by applying two consecutive superthreshold pulses with interpulse duration t_d. The second pulse, if preceded by an interpulse duration of less than a minimum duration (t_{dmin}), partially or totally fails to evoke a response, Fig. 8 *A*. This is due to a refractory region in the phase space (FitzHugh, 1961). This is consistent with experimental observation 2.8.

A "return" map is generated by plotting the ratio of response amplitudes to the first and second pulse (A2/A1) against t_d. The return maps show that t_{dmin} decreased with increasing β (Fig. 8 *B* and *C*). t_{dmin} depends on the function $F(\beta, V)$, which moves the steady state of the system on the line SS' in Fig. 2 *B*. As the steady state of the system approaches the oscillatory domain (thick section on SS'), t_{dmin} decreases due to the increased excitability of the system. Thus, depolarizing the tissue would increase the chances of evoking a full slow wave response. This is consistent with the experimental observations 2.4.

An interesting return map, Fig. 8 *C*, appears near the bistable region (see Fig. 3 and 2 *D*). For some values of t_d the trajectory is pushed closer to the basin of attraction of the nonperiodic steady state (not shown). This reduces the amplitude of the second response for most t_d and for some values of t_d, the trajectory becomes trapped in the basin of attraction, decaying to the nonperiodic steady state. Thus, a nonresponsive t_d appears in the otherwise responsive region of the return map. This behavior has not been observed in

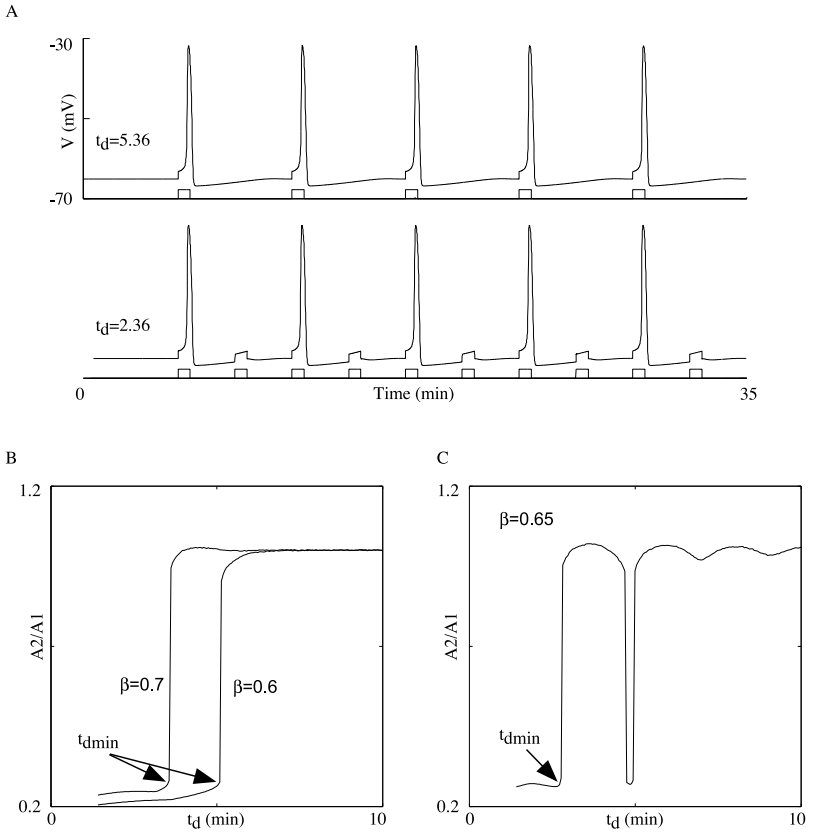

FIGURE 8 Effect of interpulse duration on current pulse induced responses. (*A*) Pulses fail to evoke responses if interpulse duration (t_d) is reduced below a critical value (t_{dmin}). Top trace is membrane potential and bottom trace is current. Traces are shown for β = 0.7 μM, for interpulse durations as labeled. (*B*) Return map shows amplitude of second pulse divided by the amplitude of the first (A2/A1) as a function of the interval between the two pulses, for two values of β. (*C*) Return map close to the bistable region with β = 0.65 μM (see Fig. 2 *D*).

the smooth muscle tissue. However, considering the narrow range of the bistable region, it is expected that this behavior would be difficult to observe.

DISCUSSION

Slow waves have been studied using two classes of models: one based on cardiac-like pacemaker voltage-dependent mechanisms (Publicover, 1995; Publicover and Sanders, 1989) and the other on coupled oscillators based synchronization of relaxation oscillators (Nelsen and Becker, 1968; Sarna et al., 1971, 1972). Recently a model based on a combination of the previous two classes has also been proposed (Aliev et al., 2000). These models have studied the propagation and electrical activity of slow waves. The aim of the current work was to investigate the mechanism underlying the excitable nature of gastric smooth muscle based on recent experimental data. The mathematical model described here was developed to qualitatively examine the role of membrane potential dependent IP_3 synthesis in the excitability of the gastric smooth muscle tissue and its role in the generation and control of slow waves.

A point most essential to our model is the underlying excitable nature of the Ca^{2+} dynamics. Preliminary results obtained by using different models (FitzHugh-Nagumo) (FitzHugh, 1961; Nagumo et al., 1964; Atri et al., 1993; De Young and Keizer, 1992; Hofer, 1999) to describe Ca^{2+} dynamics in our model were in qualitative agreement with our experimental observations. A common factor in all these models was the excitable nature of the Ca^{2+} release, which highlights the importance of excitability of the store-cytosolic Ca^{2+} system to our model. Our model demonstrates that membrane potential, acting through IP_3, can alter the excitability of the cell, and induce, abolish, and/or modulate slow wave frequency in a way that accords with experimental observations.

Membrane potential may modulate Ca^{2+} entry into the cell and changes in the cytosolic Ca^{2+} modulate IP_3 synthesis through phospholipase C activation (Fig. 1 *B*). In this case the net effect of Ca^{2+} and voltage feedback on IP_3 synthesis (Fig. 1 *B* and *C*, respectively) should be similar. However, gastric smooth muscle exhibits voltage dependent Ca^{2+} release in the presence of L-Ca^{2+} channel blockade or short-term exposure to Cd^{2+} and/or reduced external Ca^{2+} (Edwards et al., 1999; Suzuki and Hirst, 1999; van Helden et al., 2000), and hence there would be no voltage activated Ca^{2+} flux into the cell. Thus, the observed responses are likely to be due to voltage-induced IP_3 synthesis (Fig. 1 *B*) and not due to Ca^{2+}-induced IP_3 synthesis (Fig. 1 *C*).

The existence of two distinct feedback mechanisms (Fig. 1 *B* and *C*) has important physiological implications. In cells where voltage gated inward Ca^{2+} flux is available but not operative, either due to membrane potential failing to reach threshold or because voltage-gated channels have been blocked, voltage feedback would provide an effective con-

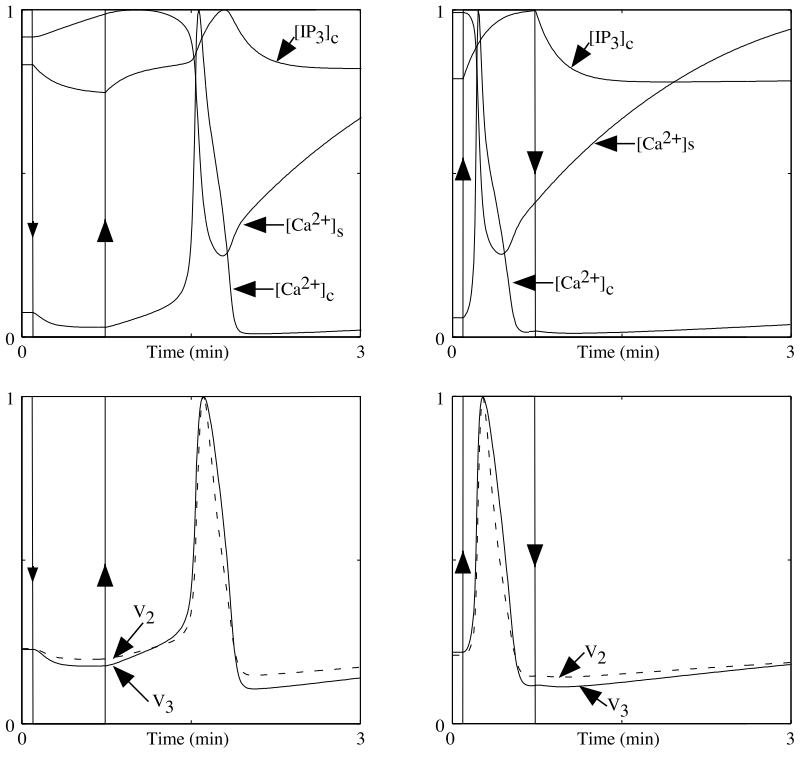

FIGURE 9 Responses to polarizing pulses. Figures in the first column show responses to a hyperpolarizing pulse. The second column shows responses to a depolarizing pulse. Arrowheads show polarity of current injection. All traces are normalized. Top row shows IP_3 concentration ($[IP_3]_c$), store ($[Ca^{2+}]_s$), and cytosolic ($[Ca^{2+}]_c$) calcium concentrations as a function of time. Bottom row shows Ca^{2+} fluxes into (V_2) and out (V_3) of the intracellular Ca^{2+} store. A hyperpolarizing (depolarizing) pulse decreases (increases) the $[IP_3]_c$, which causes a decrease (increase) in the release of Ca^{2+} from the store (V_3) as well as decreased (increased) store refilling (V_2). In the case of a hyperpolarizing pulse, the rate of refilling the store is reduced less than the rate of Ca^{2+} release, resulting in a net increase in the store $[Ca^{2+}]_s$. On return to resting membrane potential, the system becomes unstable and goes through a single oscillation.

trol of IP_3 production. In nonexcitable cells, where depolarizations do not increase Ca^{2+} influx (see Mahaut-Smith et al., 1999), or in cell types where Ca^{2+} dependent modulation of IP_3 synthesis has not been found to be operative (Bird et al., 1997), a voltage dependent IP_3 feedback mechanism would be effective in modulating Ca^{2+} dynamics through membrane potential.

Step changes in membrane potential were used to investigate the details of the dynamics underlying results from experiments where smooth muscle cells were subjected to current injection during intracellular recordings. Depending on the amplitude, duration and timing of the pulse, the response to the pulse could be either a full slow wave or a subthreshold response close to the steady state. Moreover, this voltage-dependent system was found to be bistable within a specific range of stimulation conditions.

Simulations using the model cell, which included voltage dependent IP_3 synthesis, produced changes in membrane potential followed by changes in $[IP_3]_c$ with a time delay. While the rate of IP_3 synthesis may change rapidly with changing membrane potential, it nevertheless takes some time for the $[IP_3]_c$ to increase or decrease. The full slow-wave response requires a minimum amount of $[IP_3]_c$ and so the latency of the response arises, at least in part, from the time taken for accumulation of this threshold $[IP_3]_c$. A similar explanation has been suggested by Ganitkevich and Isenberg (1993) for membrane potential modulated changes in $[IP_3]_c$ in coronary myocytes.

The responses to current pulses of positive versus negative polarities showed important differences in latencies and peak amplitudes. The latencies of responses to hyperpolarizing pulses were found to be longer than those induced by depolarizing pulses. The physiological differences between the two responses become apparent by examining the direction of initial trajectory movement in the phase space immediately after pulse injection. At the onset of a depolarizing pulse, $[IP_3]_c$ starts to increase (Fig 9). Ca^{2+} influx into the cell from the extracellular space (V_{in}) and release from the intracellular Ca^{2+} store (V_3) are both dependent on IP_3, so both start to increase as $[IP_3]_c$ increases. If this increase in Ca^{2+} reaches the threshold for CICR, a large, slow wave like response is produced.

However, the sequence of events is different for a hyperpolarizing pulse. Because there is a voltage-dependent component to IP_3 production at the resting membrane potential, upon initiation of a hyperpolarizing pulse $[IP_3]_c$ starts to decrease due to inhibition of the voltage-dependent IP_3 synthesis. As $[IP_3]_c$ decreases, Ca^{2+} entry from outside (V_{in}), and release from the intracellular Ca^{2+} store (V_3) also decreases. However, the flux that refills the store (V_2) is not dependent on IP_3, so it is not affected by this decrease in IP_3 (although it decreases due to lower $[Ca^{2+}]_c$). The result is a net increased flux of Ca^{2+} into the store. At termination of the pulse, the intracellular Ca^{2+} store is in a "supercharged" state. Even though the intracellular Ca^{2+} store is now filled, it will not release Ca^{2+} because of the low levels of Ca^{2+} and IP_3 in the cytosol ($[Ca^{2+}]_c$ and $[IP_3]_c$ are not sufficient to initiate CICR or IICR). Thus, following termination of the pulse, the state of the intracellular Ca^{2+} store remains constant, while the $[IP_3]_c$ returns to its resting level

causing the cytosol to refill with Ca^{2+} from the extracellular space (horizontal movement in phase space). Now even the former steady-state level of $[IP_3]_c$ is sufficient to initiate CICR because of the increased Ca^{2+} in the store, and a slow wave response results.

The instantaneous state of the system is dependent on the function $F(\beta, V)$, which controls the excitability of the system. As the steady state of the system approaches the oscillatory region, Fig. 2 *B*, the latency of response decreases (not shown) due to the increased excitability of the system. Increasing agonist concentration, and/or depolarizing the cell, makes the system more excitable, and thus decreases the latency of response to current pulses. This behavior is also illustrated by the return maps shown in Fig. 8. At increased IP_3 the cell is able to respond to higher frequencies of driving pulses due to increased excitability of the system.

All these results are consistent with experimental observations. Furthermore, based on the model dynamics, we were also able to predict tissue behaviors that have not yet been experimentally observed. Specifically, 1) slow waves may be induced and abolished at the upper bounds of agonist stimulation; 2) minimum pulse amplitude required to evoke a response from the tissue would depend on the agonist level; 3) latency of response would change if resting membrane potential is changed; 4) a nonresponsive region in the return map may exist at specific agonist concentrations.

CONCLUSION

A parsimonious qualitative mathematical model was developed to investigate observations made on isopotential strips of smooth muscle from guinea-pig stomach. Voltage feedback on IP_3 synthesis was postulated to be a key mechanism necessary to explain the observed responses of the tissue.

Experimental observations were successfully reproduced numerically using the model cell. A detailed analysis showed that the excitability of the tissue can be controlled by agonist application or membrane potential changes. It was demonstrated that slow wave induction and abolition by current injection exists due to the nonlinear nature of voltage-dependent IP_3 synthesis. The mathematical model provided an explanation for the experimentally observed differences in responses to hyperpolarizing and depolarizing pulses (e.g., latency of response and minimum latency of response).

Our mathematical model provides additional support for the postulated voltage dependence of IP_3 synthesis. Not only does our model provide insight into the experimental observations made on isolated tissue, but also predicts four additional behaviors that have not yet been reported. These predictions will be tested in future work to gain further insight into the dynamics of the Ca^{2+} release and slow waves.

The authors would like to thank Dr. Chris Katnik for a critical review of the manuscript. D. F. van Helden and M. S. Imtiaz were supported by The Australian Research Council, National Health and Medical Research Council of Australia, and The Hunter Heart-Lung Research Guild.

REFERENCES

Aliev, R. R., W. Richards, and J. P. Wikswo. 2000. A simple nonlinear model of electrical activity in the intestine. *J. Theor. Biol.* 204:21–28.

Atri, A., J. Amundson, D. Clapham, and J. Sneyd. 1993. A single-pool model for intracellular calcium oscillations and waves in the *Xenopus laevis* oocyte. *Biophys. J.* 65:1727–1739.

Berridge, M. J. 1993a. Cell signalling: a tale of two messengers. *Nature.* 365:388–389.

Berridge, M. J. 1993b. Inositol trisphosphate and calcium signalling. *Nature.* 361:315–325.

Best, L., and T. B. Bolton. 1986. Depolarisation of guinea-pig visceral smooth muscle causes hydrolysis of inositol phospholipids. *Naun. Schm. Arch. Pharmacol.* 333:78–82.

Bird, G. S., J. F. Obie, and J. W. Putney, Jr. 1997. Effect of cytoplasmic Ca^{2+} on (1,4,5) IP_3 formation in vasopressin-activated hepatocytes. *Cell Calcium.* 21:253–256.

Bolton, T. B. 1971. On the nature of the oscillations of the membrane potential (slow waves) produced by acetylcholine or carbachol in intestinal smooth muscle. *J. Physiol.* 216:403–418.

Daniel, E. E., B. L. Bardakjian, J. D. Huizinga, and N. E. Diamant. 1994. Relaxation oscillator and core conductor models are needed for understanding of GI electrical activities. *Am. J. Physiol.* 266:G339–G349.

De Young, G. W., and J. Keizer. 1992. A single-pool inositol 1,4,5-trisphosphate-receptor-based model for agonist-stimulated oscillations in Ca^{2+} concentration. *Proc. Natl. Acad. Sci. U.S.A.* 89:9895–9899.

Doedel, E., and J. P. Kernevez. 1986. AUTO: Software for Continuation and Bifurcation Problems in Ordinary Differential Equations. California Institute of Technology, Pasadena, CA.

Donaldson, S. K., N. D. Goldberg, T. F. Walseth, and D. A. Huetteman. 1988. Voltage dependence of inositol 1,4,5-trisphosphate-induced Ca^{2+} release in peeled skeletal muscle fibers. *Proc. Natl. Acad. Sci. U.S.A.* 85:5749–5753.

Dupont, G., M. J. Berridge, and A. Goldbeter. 1990. Latency correlates with period in a model for signal-induced Ca^{2+} oscillations based on Ca^{2+} -induced Ca^{2+} release. *Cell. Regul.* 1:853–861.

Dupont, G., and C. Erneux. 1997. Simulations of the effect of inositol 1,4,5-trisphosphate 3-kinase and 5-phosphatase activities on Ca^{2+} oscillations. *Cell Calcium.* 22:321–331.

Dupont, G., and A. Goldbeter. 1993. One-pool model for Ca^{2+} oscillations involving Ca^{2+} and inositol 1,4,5-trisphosphate as co-agonists for Ca^{2+} release. *Cell Calcium.* 14:311–322.

Edelstein-Keshet, L. 1988. Mathematical Models in Biology. McGraw-Hill.

Edwards, F. R., G. D. Hirst, and H. Suzuki. 1999. Unitary nature of regenerative potentials recorded from circular smooth muscle of guinea-pig antrum. *J. Physiol.* 519:235–250.

Ermentrout, B. 1994. XPPAUT-The Differential Equations Tool. Available at ftp://ftp.math.pitt.edu.au/pub/bardware/. Last accessed August 22, 2002.

FitzHugh, R. 1961. Impulses and physiological states in theoretical models of nerve membrane. *Biophys. J.* 1:445–466.

Ganitkevich, V. Y., and G. Isenberg. 1993. Membrane potential modulates inositol 1,4,5-trisphosphate-mediated Ca^{2+} transients in guinea-pig coronary myocytes. *J. Physiol.* 470:35–44.

Ganitkevich, V. Y., and G. Isenberg. 1996. Effect of membrane potential on the initiation of acetylcholine-induced Ca^{2+} transients in isolated guinea pig coronary myocytes. *Circ. Res.* 78:717–723.

Harootunian, A. T., J. P. Kao, S. Paranjape, S. R. Adams, B. V. Potter, and R. Y. Tsien. 1991a. Cytosolic Ca^{2+} oscillations in REF52 fibroblasts: Ca^{2+}-stimulated IP_3 production or voltage-dependent Ca^{2+} channels as key positive feedback elements. *Cell Calcium.* 12:153–164.

Harootunian, A. T., J. P. Kao, S. Paranjape, and R. Y. Tsien. 1991b. Generation of calcium oscillations in fibroblasts by positive feedback between calcium and IP_3. *Science.* 251:75–78.

Hashitani, H., D. F. Van Helden, and H. Suzuki. 1996. Properties of spontaneous depolarizations in circular smooth muscle cells of rabbit urethra. *Br. J. Pharm.* 118:1627–1632.

Hirose, K., S. Kadowaki, M. Tanabe, H. Takeshima, and M. Iino. 1999. Spatiotemporal dynamics of inositol 1,4,5-trisphosphate that underlies complex Ca^{2+} mobilization patterns. *Science.* 284:1527–1530.

Hofer, T. 1999. Model of intercellular calcium oscillations in hepatocytes: synchronization of heterogeneous cells. *Biophys. J.* 77:1244–1256.

Houart, G., G. Dupont, and A. Goldbeter. 1999. Bursting, chaos and birhythmicity originating from self-modulation of the inositol 1,4,5-trisphosphate signal in a model for intracellular Ca^{2+} oscillations. *Bull. Math. Biol.* 61:507–530.

Huang, S., S. Nakayama, S. Iino, and T. Tomita. 1999. Voltage sensitivity of slow wave frequency in isolated circular muscle strips from guinea pig gastric antrum. *Am. J. Physiol.* 276:G518–G528.

Itoh, T., N. Seki, S. Suzuki, S. Ito, J. Kajikuri, and H. Kuriyama. 1992. Membrane hyperpolarization inhibits agonist-induced synthesis of inositol 1,4,5-trisphosphate in rabbit mesenteric artery. *J. Physiol.* 451: 307–328.

Keizer, J., and G. De Young. 1993. Effect of voltage-gated plasma membrane Ca^{2+} fluxes on IP_3-linked Ca^{2+} oscillations. *Cell Calcium.* 14: 397–410.

Liu, L. W., L. Thuneberg, and J. D. Huizinga. 1995. Cyclopiazonic acid, inhibiting the endoplasmic reticulum calcium pump, reduces the canine colonic pacemaker frequency. *J. Pharm. Exp. Therap.* 275:1058–1068.

Mahaut-Smith, M. P., J. F. Hussain, and M. J. Mason. 1999. Depolarization-evoked Ca^{2+} release in a non-excitable cell, the rat megakaryocyte. *J. Physiol.* 515:385–390.

Mason, M. J., J. F. Hussain, and M. P. Mahaut-Smith. 2000. A novel role for membrane potential in the modulation of intracellular Ca^{2+} oscillations in rat megakaryocytes. *J. Physiol.* 524:437–446.

Mason, M. J., and M. P. Mahaut-Smith. 2001. Voltage-dependent Ca^{2+} release in rat megakaryocytes requires functional IP_3 receptors. *J. Physiol.* 533:175–183.

Meyer, T., and L. Stryer. 1991. Calcium spiking. *Annu. Rev. Biophys. Biophys. Chem.* 20:153–174.

Nagumo, J., S. Arimoto, and S. Yoshizawa. 1964. An active pulse transmission line simulating nerve axon. *Proc. IRE.* 50:2061–2070.

Nelsen, T. S., and J. C. Becker. 1968. Simulation of the electrical and mechanical gradient of the small intestine. *Am. J. Physiol.* 214:749–757.

Nose, K., H. Suzuki, and H. Kannan. 2000. Voltage dependency of the frequency of slow waves in antrum smooth muscle of the guinea-pig stomach. *Jpn. J. Physiol.* 50:625–633.

Prosser, C. L., and A. W. Mangel. 1982. Cellular Pacemakers. John Wiley and Sons, New York.

Publicover, N. G. 1995. Generation and propagation of rhythmicity in gastrointestinal smooth muscle. *In* Pacemaker Activity and Intercellular Communication. JD Huizinga, editor. Ann Arbor, MI CRC. 175–190.

Publicover, N. G., and K. M. Sanders. 1989. Are relaxation oscillators an appropriate model of gastrointestinal electrical activity? *Am J. Physiol.* 256:G265–274.

Sanders, K. M. 1996. A case for interstitial cells of Cajal as pacemakers and mediators of neurotransmission in the gastrointestinal tract. *Gastroenterology.* 111:492–515.

Sarna, S. K., E. E. Daniel, and Y. J. Kingma. 1971. Simulation of slow-wave electrical activity of small intestine. *Am. J. Physiol.* 221:166–175.

Sarna, S. K., E. E. Daniel, and Y. J. Kingma. 1972. Simulation of the electric-control activity of the stomach by an array of relaxation oscillators. *Am. J. Dig. Dis.* 17:299–310.

Sneyd, J., S. Girard, and D. Clapham. 1993. Calcium wave propagation by calcium-induced calcium release: an unusual excitable system. *Bull. Math. Biol.* 55:315–344.

Suzuki, H., and G. D. Hirst. 1999. Regenerative potentials evoked in circular smooth muscle of the antral region of guinea-pig stomach. *J. Physiol.* 517:563–573.

Takazawa, K., M. Lemos, A. Delvaux, C. Lejeune, J. E. Dumont, and C. Erneux. 1990. Rat brain inositol 1,4,5-trisphosphate 3-kinase. Ca^{2+}-sensitivity, purification and antibody production. *Biochem. J.* 268: 213–217.

Tomita, T. 1981. Electrical activity (spikes and slow waves) in gastrointestinal smooth muscles. *In* Smooth Muscle: An Assessment of Current Knowledge. E Bulbring, AF Brading, AW Jones, T Tomita, editors. University of Texas Press. Austin, TX. p 127–156.

van Helden, D. F., M. S. Imtiaz, K. Nurgaliyeva, P. von der Weid, and P. J. Dosen. 2000. Role of calcium stores and membrane voltage in the generation of slow wave action potentials in guinea-pig gastric pylorus. *J. Physiol.* 524:245–265.

Vergara, J., R. Y. Tsien, and M. Delay. 1985. Inositol 1,4,5-trisphosphate: a possible chemical link in excitation-contraction coupling in muscle. *Proc. Natl. Acad. Sci. U.S.A.* 82:6352–6356.

Yamagishi, T., T. Yanagisawa, and N. Taira. 1992. K+ channel openers, cromakalim and Ki4032, inhibit agonist-induced Ca^{2+} release in canine coronary artery. *Naun. Schm. Arch. Pharmacol.* 346:691–700.